THE JOURNAL OF PHYSICAL CHEMISTRY LETTERS
A JOURNAL OF THE AMERICAN CHEMICAL SOCIETY

pubs.acs.org/JPCL Letter

Octahedra-Tilted Control of Displacement Disorder and Dielectric Relaxation in Mn-Doped $SrTiO_3$ Single Crystals

Mikhail V. Talanov,* Adam I. Stash, Sergey A. Ivanov, Elena S. Zhukova, Boris P. Gorshunov, Boris M. Nekrasov, Vasily S. Stolyarov, Vladislav I. Kozlov, Maxim Savinov, and Alexander A. Bush

Cite This: *J. Phys. Chem. Lett.* 2022, 13, 11720−11728 Read Online

ACCESS | Metrics & More | Article Recommendations | Supporting Information

ABSTRACT: Strontium titanate $SrTiO_3$ (STO) is a canonical example of a quantum paraelectric, and its doping with manganese ions unlocks its potential as a quantum multiferroic candidate. However, to date, the specifics of incorporation of the manganese ion into the perovskite lattice and its impact on structure−property relationships are debatable questions. Herein, using high-precision X-ray diffraction of a Mn (2 atom %)-doped STO single crystal, clear fingerprints of the displacement disorder of Mn cations in the perovskite B-sublattice are observed. Moreover, near the temperature of the antiferrodistortive transition, the off-center Mn position splits in two, providing the unequal potential barrier's distribution for possible local atomic hopping. A link with this was found via analysis of the dielectric response that reveals two Arrhenius-type relaxation processes with similar activation energies (35 and 43 meV) and attempt frequencies (1×10^{11} and $\sim 1.6 \times 10^{10}$ Hz), suggesting similar dielectric relaxation mechanisms.

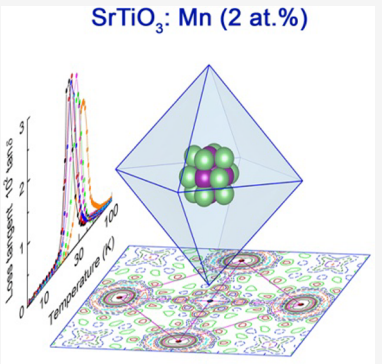

Strontium titanate $SrTiO_3$ (STO) is a perovskite-type material that demonstrates incipient ferroelectric behavior and a quantum paraelectric low-temperature state.[1,2] It is believed that zero-point quantum fluctuations preclude the condensation of the polar soft mode and a macroscopic ferroelectric state does not form down to the millikelvin range.[1,2] At the same time, the dielectric permittivity reaches $\sim 10^4$ without significant dispersion in the microwave frequency range,[3] which is attractive for application in various types of tunable electronic devices,[4,5] nanotechnology,[6,7] and photocatalysis.[8,9] At ∼105−110 K, STO undergoes an antiferrodistortive transition to a nonferroelectric tetragonal phase formed by out-of-phase tilts of oxygen octahedra.[10,11] This improper ferroelastic $Pm\bar{3}m \rightarrow I4/mcm$ phase transition has an intermediate nature between second-order and tricritical[12] and is characterized by ultralow values of the order parameter (tilting angle of ∼2° at 1.5 K).[13,14] Despite this, the symmetry lowering through the phase transition leads to splitting of the polar soft mode (F_{1u}) into two components (E_u and A_{2u})[15] and to the appearance of locally polar ferroelastic twin walls[16,17] remaining highly mobile down to low temperatures.[18] Moreover, the competition between ferroelectric and antiferrodistortive instabilities (and accompanying strains) can have an even greater impact on the suppression of the polar state than quantum fluctuations.[15,19]

There are several ways to induce the ferroelectric state in STO, including (i) application of strong dc[20] or terahertz-pulse electric fields,[21] (ii) application of uniaxial pressure,[22] (iii) misfit strain in thin films,[23] (iv) oxygen isotope exchange,[24] (v) formation of defect/defect complexes,[25,26] and (vi) iso- or heterovalent cation substitution.[27−31] In the latter case, different types of polar behavior that depend on the substituted sublattice, impurity ion, and its concentration are observed. At the same time, it was found that substitution of Sr (especially with Ca, Ba, or Pb) has a more pronounced effect on the dielectric properties compared to substitution of Ti.[32] Special attention is given to doping STO with magnetic impurities of 3d transition elements to achieve multiferroic behavior, which greatly expands the material's functionality via the possible magnetic-field control of its dielectric properties. Shvartsman et al.[33] showed that substitution of Sr with Mn^{2+} (2 mol %) in the A sublattice leads to freezing of both spin and dipole systems at 34 and 38 K, respectively. As a result, an unusual multiglass state occurs with large higher-order magnetoelectric coupling between two glass systems. However, some work has criticized the proposed multiglass behavior, attributing observed spin freezing to extrinsic contributions in ceramics, in particular, to Mn_3O_4 impurities or the nonrandom distribution of Mn^{2+} and Mn^{4+} ions.[34−36] The study of Mn-doped STO is particularly important in light of the concept of multiferroic quantum criticality, which combines magnetic and ferroelectric quantum critical behavior in the same system.[37]

Received: November 18, 2022
Accepted: December 7, 2022

https://doi.org/10.1021/acs.jpclett.2c03513
J. Phys. Chem. Lett. 2022, 13, 11720−11728

The multivalence of Mn ions and the similarity of their ionic radii to those of Sr^{2+} and Ti^{4+} (Table S1) allow their incorporation into both A and B perovskite sublattices with various Mn valence states (2+, 3+, and 4+) and diverse defect formation schemes depending on the processing conditions.[34−36,38−41] In particular, for ceramic samples, sintering in oxygen results in the incorporation of Mn^{4+} at Ti positions while firing in a reducing atmosphere leads to the preferable substitution of Sr with Mn^{2+}.[42] Solid solutions of $Sr_{1-x}Mn_xTiO_3$ and $SrTi_{1-x}Mn_xO_3$ have different solubility limits of 3% and 15%, respectively,[43] as well as various impacts of Mn doping on the soft mode behavior and low-frequency dielectric response.[44] However, as shown by Savinov et al.,[45] A- and B-substituted ceramics with a low Mn concentration (0.1 atom %), as well as STO:Mn (0.1 atom %) single crystals, demonstrate similar low-temperature dielectric relaxation processes with almost the same values of the Arrhenius fitting parameters. The low-temperature dielectric relaxation in Mn-doped STO is explained by two types of models: temperature-activated hopping of Mn ions that randomly occupy off-center positions and reorientation of defects associated with $Mn^{2+}_{Ti}-O-$ polaronic centers.[42,45−48] However, they are characterized by the relatively similar activation energies (E_a) and attempt frequencies (f_0), which prevents the establishment of the relaxation mechanism based on the dielectric data only (see Table S2 for a review). According to the electron spin resonance (ESR)[38] and X-ray absorption fine structure measurements,[49,50] Mn^{2+} ions occupy off-center positions strongly (by 0.77 Å) displaced along the ⟨001⟩ direction from the central Sr site. Parameters E_a and f_0 from the ESR are in a good agreement with dielectric data that evidently confirm the off-center Mn hopping as the origin of the low-temperature relaxation.[38] At the same time, it is believed that in B-substituted STO Mn^{4+} ions occupy the central position that prevents local dipole formation (see, for example, refs 45, 50, and 51). Moreover, Tkach et al.[48] noted that B substitution does not induce low-temperature dielectric relaxation, which is characteristic of A-substituted ceramics with low concentrations of Mn (several atomic percent). However, studies of Mn localization in B-substituted STO and its dielectric properties have been carried out on different samples (ceramics and crystals) at various dopant concentrations, which complicate the establishment of the possible origin of dielectric relaxation.

In this Letter, on the basis of the results of precise X-ray single-crystal diffraction, we show for the first time that at room temperature Mn ions in $SrTi_{1-x}Mn_xO_3$ occupy positions displaced along the ⟨001⟩ direction by 0.31 Å, which allows manifestation of the off-center Mn hopping and related dielectric relaxation. Moreover, at temperatures near the antiferrodistortive transition, the randomly occupied off-center position splits into two other crystallographically non-equivalent off-center positions. This provides the specific potential barrier distribution for local hopping of Mn ions, which explains the experimental observation of the two dielectric relaxation processes with similar Arrhenius fitting parameters.

Panels a and b of Figure 1 show the reciprocal space projections obtained for the 296 and 100 K data at the same diffractometer angle settings for the STO:Mn (2 atom %) single crystal. One can see that cooling to 100 K does not lead to the appearance of any superstructural reflections, which could indicate a known antiferrodistortive phase transition

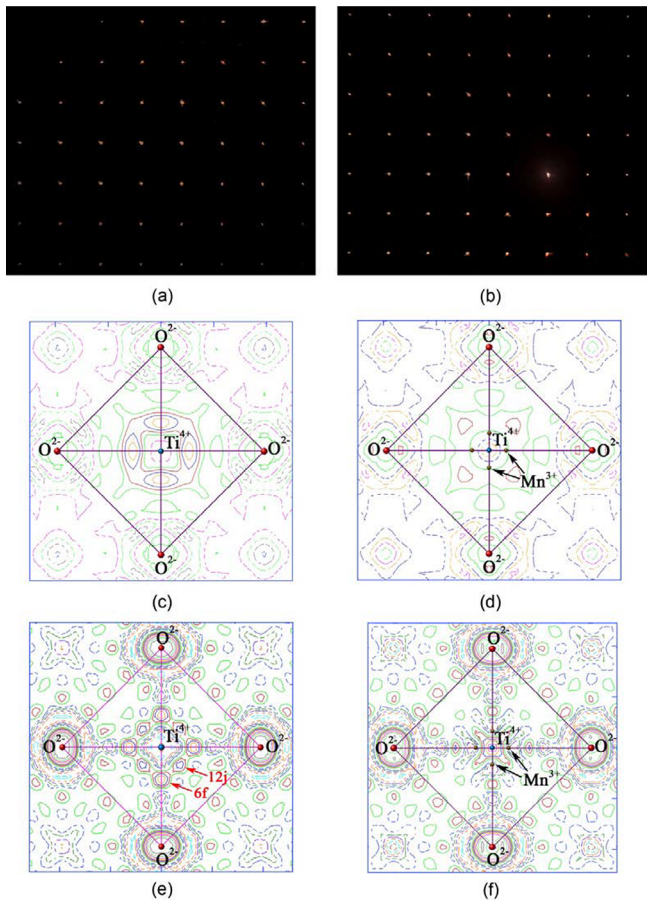

Figure 1. (a and b) Reciprocal space diffraction peaks obtained by pixel-by-pixel conversion of 1200 experimental frames, measured for a STO:Mn single crystal at 296 and 100 K, respectively. Panels a and b show projections in the [1 0 0] plane. Residual electron density of a STO:Mn single crystal (c and e) without and (d and f) with Mn^{3+} cation at (c and d) 296 K and (e and f) 100 K. Negative isolines are marked with dotted lines, and positive ones with solid lines. The isoline step is 0.1 e/Å^3.

from the cubic phase ($Pm\bar{3}m$) to the tetragonal one ($I4/mcm$). Precise low-temperature experiments (Table 1) showed that within the accuracy of the experiment, no deviations from cubic symmetry were observed. At the same time, an attempt was made to refine the structure in the tetragonal $I4/mcm$ space group. Despite the increase in the number of refined parameters, the quality criteria turned out to be worse and the refinement process did not allow us to obtain physically significant results. However, the temperature dependencies of the cubic (pseudocubic) unit cell parameter for both pure STO and STO:Mn single crystals demonstrate a significant deviation from linear behavior at ≈105 and ≈110 K, respectively (Figure S1). This can be interpreted as traces of the antiferrodistortive phase transition (difficulties in its direct observation by X-ray diffraction methods are discussed below).

The cubic unit cell parameter of the STO:Mn single crystal is 3.90663(3) Å. Refinement of the occupancies of the cationic and anionic positions in $SrTiO_3$ showed that the nearly ideal stoichiometry is observed only in the Sr^{2+} sublattice [0.9989(6)], while the Ti^{4+} [0.967(3)] and oxygen [0.988(9)] sublattices are characterized by the difference from the theoretical values. To determine the position of the Mn cation, during the first stage, we refined the $SrTiO_3$

https://doi.org/10.1021/acs.jpclett.2c03513
J. Phys. Chem. Lett. 2022, 13, 11720−11728

Table 1. Parameters from the X-ray Diffraction Experiment and Final Results of Crystal Structure Refinements for STO:Mn (2 atom %) and Pure STO Single Crystals

	$SrTi_{1-x}Mn_xO_{3-y}$		$SrTiO_3$	
Crystal Data				
temperature (K)	296(2)	100(2)	293(2)	90(2)
chemical formula weight M_r	183.38		183.48	
crystal system, space group	cubic, $Pm\bar{3}m$			
no. of formula units (Z)	1			
a (Å)	3.90663(3)	3.89695(5)	3.90410(6)	3.89761(5)
V (Å^3)	59.622(1)	59.180(2)	59.506(3)	59.210(2)
radiation type, wavelength λ	Mo Kα, λ = 0.71073 Å			
absorption coefficient μ (mm^{-1})	25.48	25.242	25.47	25.60
crystal size	0.134 mm × 0.094 mm × 0.077 mm		0.114 mm × 0.080 mm × 0.066 mm	
Data Collection				
diffractometer	Bruker APEXII CCD with PHOTON II detector		Bruker QUEST D8 with PHOTON III detector	
sin θ/λ (Å^{-1}) (min/max)	5.21/47.17	5.23/57.74	5.22/44.35	5.23/57.73
absorption correction	Numerical (SADABS2016/2; Bruker, 2019)			
T_{min}, T_{max}	0.211−0.442	0.136−0.321	0.192−0.409	0.192−0.438
no. of measured, independent, and observed [$I > 2\sigma(I)$] reflections	3640, 82, 80	10137, 119, 119	2665, 74, 74	5075, 119, 199
R_{int}	0.0199	0.0325	0.0196	0.0281
Structure Refinement				
$R[F^2 > 2\sigma(F^2)]$, $wR(F^2)$, GOF	0.0097, 0.0231, 1.193	0.0111, 0.0294, 1.252	0.0092, 0.0230, 1.245	0.0116, 0.0311, 1.172
no. of reflections	82	119	74	119
no. of parameters	10	7	6	6
$\Delta\rho_{max}/\Delta\rho_{min}$(e Å^{-3})	0.358/−0.341	1.091/−0.702	0.338/−0.420	1.161/−0.787
extinction coefficient	0.103(16)	0.077(17)	0.090(15)	0.057(18)
occupations (x, y)[a]	0.03(2),0.02(1)		–	

[a]According to the results of refinement of the occupations of Ti/Mn and O atoms at 296 K.

structure and built a map of the residual electron density (Figure 1c). One can see that in the Wyckoff positions 6f ($^1/_2$, x, $^1/_2$) the electron density maxima are observed 0.518 Å from the Ti^{4+} cation. Then, we positioned the Mn cation at the displaced position, determined its adjusted parameter (x = 0.42) and its occupancy (as equiprobably disordered over six positions around the Ti^{4+} cation), and carried out the final refinement of the structure with the refinement of the occupancies of the positions of the Ti^{4+} and Mn cations and the O^{2-} anion. The refinement results showed that Mn Wyckoff position 6f is shifted by 0.31 Å from the Ti^{4+} cations (occupied Wyckoff position 1b) and its occupancy is approximately 3%. This agrees well with the assumption that the Ti^{4+} cation is replaced with Mn with a slight oxygen deficiency (occupancy of 99.0%). Figure 1d shows a map of the residual electron density after refinement of the STO:Mn structure with the disordered displacement of Mn cations. The peaks of residual density in Wyckoff position 6f ($^1/_2$, x, $^1/_2$) are no longer present.

As in the case of the structure at room temperature, at the first stage the structure at 100 K was refined without Mn and a residual density map was built (Figure 1e). Note that in addition to the maxima in Wyckoff position 6f ($^1/_2$, x, $^1/_2$) that were observed at room temperature, new peaks appeared in the Wyckoff position 12j ($^1/_2$, y, y). That is, if at room temperature the Mn cation was disordered over six symmetrically equivalent positions (the occupancy of each position is $^1/_6$), then at 100 K there are apparently 18 symmetrically nonequivalent positions (6 + 12), and the occupancy of each position decreases by an additional 3 times. For this reason, it was not possible to refine the positional and thermal parameters of Mn, and the structure at 100 K was refined only without the Mn cation due to critical correlations.

It is essential to note the following specific features of the $Pm\bar{3}m \rightarrow I4/mcm$ phase transition in $SrTiO_3$, which prevent its reliable identification by X-ray diffraction methods directly near the transition temperature.

(i) Out-of-phase octahedral tilts associated with the antiferrodistorsion transition include only oxygen displacements that are difficult to detect by X-ray diffraction.

(ii) An ultralow value of the tilting angle (2°) at 1.5 K was found according to the neutron diffraction data.[13] Using group theoretical analysis, we estimate the total distortion amplitude associated with the proper order parameter R_5^- (out-of-phase octahedral tilts) as only 0.11 Å (Tables S3 and S4),[52] which is several times

https://doi.org/10.1021/acs.jpclett.2c03513
J. Phys. Chem. Lett. 2022, 13, 11720−11728

smaller than other types of distortions in perovskites.[52−54]

(iii) The phase transition has a second-order (close to a tricritical point) nature with a smooth temperature behavior of the order parameter.[12] This means that, near the phase transition temperature, the distortions are very small upon cooling by several degrees, in contrast to the first-order transition with an abrupt increase in the order parameter amplitude.

(iv) Strong anharmonicity of the atomic displacements is observed for all atoms at 145 K.[55,56]

Although the analysis of X-ray single-crystal diffraction does not reveal a clear symmetry reduction, the distribution of the residual electron density shows significant changes in the position of the Mn atoms upon cooling to 100 K (Figure 1c−f). Moreover, crystallographic analysis clearly shows that the $Pm\bar{3}m \rightarrow I4/mcm$ phase transition (Figure 2a,b) leads to

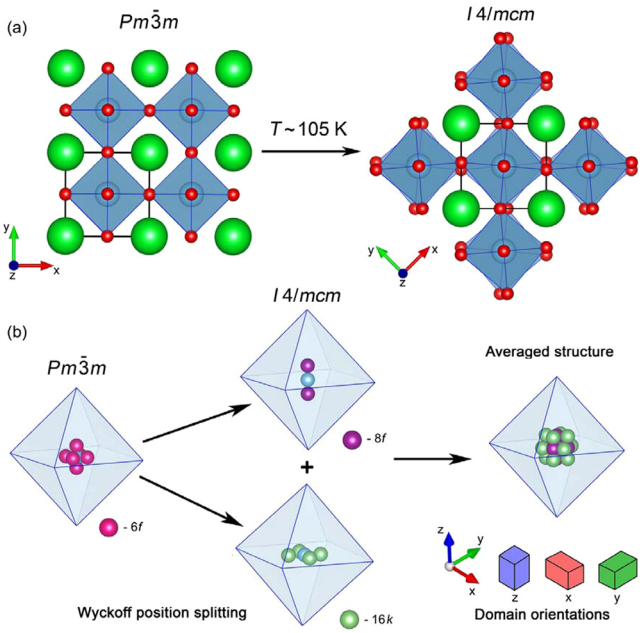

Figure 2. (a) Antiferrodistortive $Pm\bar{3}m \rightarrow I4/mcm$ phase transition in STO. Sr atoms are colored green, Ti atoms blue, and O atoms red. (b) Displacive disorder of the Mn atoms in phases with space groups $Pm\bar{3}m$ and $I4/mcm$. Wyckoff position splitting at the structural phase transition and the averaged pseudocubic structure correspond to the superposition of the Wyckoff positions in structural domains with three possible orientations of the long axis.

Wyckoff position splitting $6f$ ($^1/_2$, x, $^1/_2$) → $8f$ ($^1/_2$, $^1/_2$, z) + $16k$ (y, x, $^1/_2$) (Table S5).[57,58] The first position is moved to oxygen along the tetragonal axis, and the second is moved into a space between two oxygens (depending on the values of the adjusted parameters). Considering the formation of structural domains with different orientations of order parameter R_5^- (six structural domains with three possible orientations of the long axis), these splitting positions in the $I4/mcm$ structure can be presented as the sum of positions $6f$ ($^1/_2$, x, $^1/_2$) (Figure 1c) and $12j$ ($^1/_2$, y, y) (Figure 1d) in the averaged pseudocubic structure that corresponds to the distribution of residual electron density at 100 K (Figure 1c,d). Thus, the observed redistribution of the residual electron density at 100 K can be an indicator of the $Pm\bar{3}m \rightarrow I4/mcm$ phase transition, which cannot be reliably established on the basis of profile analysis for the reasons noted above. More significant is the fact that the observed off-center displacement of Mn ions provides the multiminimum energy profile for possible atomic hopping between crystallographically equivalent positions as a possible origin of the dielectric relaxation discussed in the literature.[42,45−48] At the same time, octahedra tilt-induced splitting of the off-center position into two crystallographically nonequivalent positions leads to the emergence of an unequal potential barrier distribution for possible local hopping of Mn ions. As a result, a more complex pattern of dielectric relaxation is expected.

Figure 3 presents the temperature dependencies of the dielectric permittivity and loss tangent of the STO:Mn single crystal measured at different frequencies in the range of 1 kHz to 1 MHz. The temperature behavior of the real permittivity (Figure 3a) demonstrates typical features observed in pure STO. $\varepsilon'(T)$ increases upon cooling, reaching values of $\varepsilon' \approx 7300$ at the lowest temperatures without revealing any anomaly related to the ferroelectric phase transition. The increase is connected purely with the temperature evolution of the ferroelectric soft mode observed at terahertz frequencies (Figure S2) whose dielectric contribution values $\Delta\varepsilon_{SM}(T)$ (blue dots in Figure 3a) practically coincide with the measured radiofrequency (RF) permittivity. At high temperatures, the dependence of RF permittivity $\varepsilon'(T)$ and dielectric contribution $\Delta\varepsilon_{SM}(T)$ of the terahertz soft mode obey Curie−Weiss behavior (inset of Figure 3a,c): $\Delta\varepsilon_{SM}(T) = \frac{C}{T - T_C}$. Soft mode frequency $\nu_{SM}(T)$ follows the Cochran law (see Figure 3d): $\nu_{SM}(T) = \text{const}\sqrt{T - T_C}$. Below 80−100 K, a strong deviation in $\varepsilon'(T)$ from Curie−Weiss dependence is observed due to suppression of the phase transition by quantum fluctuations; the temperature dependence of RF permittivity at all measured temperatures is described well by the Barrett expression[59] (inset of Figure 3a): $\varepsilon'(T) = \frac{C}{\frac{T_1}{2}\coth\frac{T_1}{2T} - T_C}$. The obtained parameters are the Curie−Weiss temperature (T_C = 31 K), the Curie−Weiss constant ($C = 8 \times 10^4$ K), and the quantum temperature (T_1 = 84 K). Similar behavior of the low-frequency permittivity and soft mode was observed for pure STO single crystals with the values of the parameters being similar to those obtained here (see, e.g., ref 1): $C = 8 \times 10^4$ K, T_1 = 80 K, and T_C = 35.5 K. This indicates no strong effect of Mn doping on the suppression of the ferroelectric instability. The pronounced peak is observed in the dielectric loss tan $\delta(T)$ that shifts from ∼20 to ∼40 K as the frequency increases from 1 kHz to 1 MHz (Figure 3b). An additional anomaly is detected at higher temperatures as a shoulder (left inset of Figure 3b), which can be associated with a second relaxation peak observed earlier in Mn-doped STO.[45] Both relaxations demonstrate the Arrhenius temperature behavior of peak frequency $\sim f_0 \exp(-E_a/k_BT)$ (here k_B is the Boltzmann constant) with an activation energy and preexponential factor (attempt frequency) for the intensive peak of 35 meV and 1×10^{11} Hz, respectively. For the weaker peak, the activation energy and preexponential factor can be estimated to be 43 meV and 1.6×10^{10} Hz, respectively.

The observed behavior of dielectric loss fundamentally differs from that typically revealed by pure STO[56] and some Mn-doped STO ceramics and crystals at temperatures of ∼60−120 K.[40−43] They are characterized by significantly higher values of E_a (∼120 meV) and are usually associated with the effects of the antiferrodistortive phase transition, in

https://doi.org/10.1021/acs.jpclett.2c03513
J. Phys. Chem. Lett. 2022, 13, 11720−11728

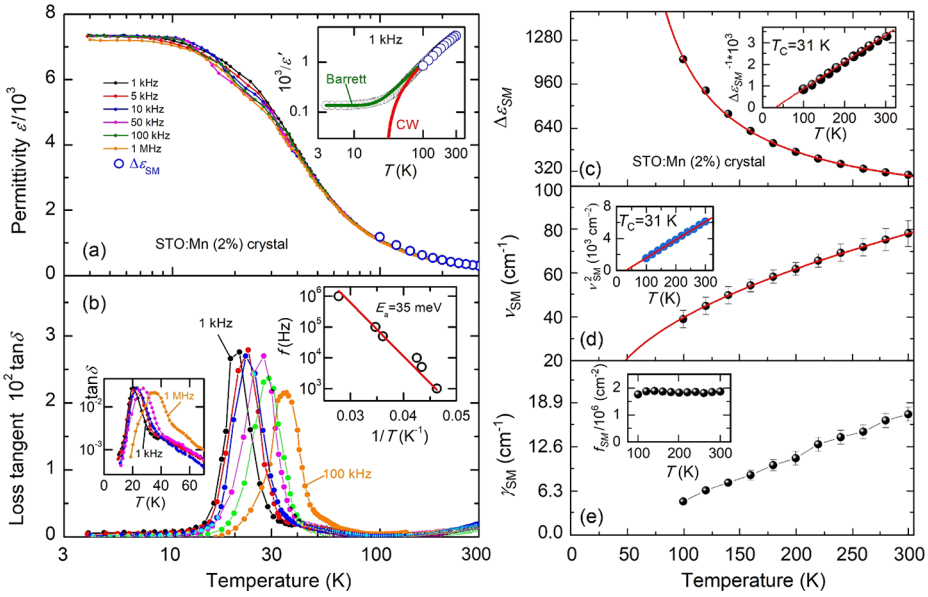

Figure 3. Temperature dependence of dielectric parameters and soft mode parameters of the $SrTiO_3$ single crystal doped with Mn (2 atom %) measured at different frequencies in the RF and terahertz ranges. (a) Temperature dependence of real RF dielectric permittivity ε' measured at several frequencies. Blue dots correspond to temperature-dependent dielectric strengths of the terahertz soft mode (see Figure S2). The inset shows the temperature dependence of the inverse RF permittivity at 1 kHz (black dots) and the inverse dielectric strength of the terahertz soft mode (blue dots). Solid lines show results of least-squares fits with Barrett and Curie–Weiss expressions with a Curie constant C of 8×10^4 K, a Curie temperature T_C of 31 K, and a quantum temperature T_1 of 84 K. (b) Temperature dependence of the loss tangent measured at several frequencies. The left inset shows that two peaks are observed with significantly different intensities. As seen in the right inset, the more intense peak displays activated temperature behavior (straight line) with an activation energy E_a of 35 meV and a preexponential factor (attempt frequency) f_0 of 1×10^{11} Hz. For the second weaker relaxation peak, the activation energy and preexponential factor can be estimated to be 43 meV and 1.6×10^{10} Hz, respectively. Temperature dependencies of the parameters of the ferroelectric soft mode observed in terahertz spectra (see Figure S2): (c) dielectric strength $\Delta\varepsilon_{SM}$, (d) frequency ν_{SM}, and (e) damping γ_{SM} (see eq S1). The insets of panels c and d show the temperature dependencies of the soft mode inverse dielectric strength and squared frequency, respectively. Straight lines in these insets correspond to the Curie–Weiss and Cochran laws with a Curie constant C of 8×10^4 K and a Curie temperature T_C of 31 K. The inset of panel e shows the temperature-independent soft mode oscillator strength $f_{SM} = \Delta\varepsilon_{SM}\nu_{SM}^2$.

particular, with the dynamics of ferroelastic domain walls.[45,60] As noted by us earlier, the origin of the low-temperature dielectric relaxation in Mn-doped STO crystals and in ceramics is discussed in terms of possible temperature-activated hopping of Mn ions and reorientation of the polarons connected with defect centers Mn^{2+}_{Ti}–O–, which have similar values of E_a and f_0.[42,45−48] For A- substituted STO (Mn^{2+} substitutes for Sr^{2+}), the results of ESR[38] and XAD[49,50] strongly argue for off-center Mn^{2+} positions, and as a consequence, a Mn hopping mechanism is preferred. On the contrary, there was no evidence of the off-center positions for Mn in B-substituted STO (Mn^{4+} substitutes for Ti^{4+}); according to the analysis of XANES and EXAFS spectra[50] as well as density functional theory calculations,[51] the dielectric relaxation is usually associated with the polaronic mechanisms.[42,45−48] On the basis of our results, we summarize the experimental facts that allow us to put forward the more likely mechanism of dielectric relaxation in STO:Mn single crystals.

(i) According to the results of highly accurate ($R \sim 1\%$; GOF ~ 1.2) single-crystal diffraction, the noncentral position of Mn ions in the B sublattice was established.

(ii) It was shown that at temperatures near the antiferrodistortive transition the randomly occupied off-center position splits into two crystallographically nonequivalent off-center positions, providing the specific potential barriers for possible local hopping of Mn ions. This correlates well with the two observed RF relaxation processes detected at 20–60 K, i.e., below the temperature of the antiferrodistortive transition.

(iii) The relaxation processes are characterized by similar activation energies (38 and 43 meV) and attempt frequencies (10^{11} and ~1.6×10^{10} Hz); the corresponding loss anomalies manifest at similar temperatures, but they have different intensities, suggesting the same physical mechanism for the two relaxations.

(iv) Similar dielectric behavior with two coexisting relaxation processes was observed in studies of B-substituted STO:Mn ceramics[45] and single crystals with a significantly lower Mn concentration (0.1 atom %) in the same temperature range.

(v) According to Lemanov et al.,[46] the temperature dependencies of the relaxation frequency in STO-based ceramics deviate from Arrhenius behavior at <10 K. This deviation is described well by accounting for the quantum tunneling regime with a barrier width of 0.3 Å (for B-substituted STO:Mn ceramics), which is very similar to the displacement of the Mn atomic positions (0.31 Å) established by us on the basis of single-crystal diffraction.

Note that considering only results iii–v does not allow us to give preference to any of the two possible relaxation mechanisms, hopping or polaronic. However, the discovered off-center positions of Mn in the B sublattice and their correlation with the features of the dielectric RF response present a strong argument in favor of temperature-activated

https://doi.org/10.1021/acs.jpclett.2c03513
J. Phys. Chem. Lett. 2022, 13, 11720−11728

hopping of Mn as the origin of dielectric relaxation in STO:Mn crystals.

We emphasize that displacement disorder is usually observed for cations having a strong electronic tendency to noncentrosymmetric coordination. Typical examples are cations Bi^{3+} and Pb^{2+} with a stereochemically active lone pair of electrons in perovskites,[61,62] pyrochlores,[63−65] and hexaferrites[66] or transition metals with a d^0-electronic configuration enabling the pseudo-Jahn−Teller effect like Ti^{4+} in $BaTiO_3$.[67] In systems with a d^n-electronic configuration, the pseudo-Jahn−Teller effect may arise from the balance between vibronic coupling and low rigidity, as well as the energy gap between the ground and excited states.[68,69] For STO:Mn, the situation becomes more complicated due to the multivalence states of manganese (2+, 3+, and 4+), which can be present in different forms (with or without charge-compensated vacancies) at various substitution schemes under the external condition.[34−36,38−41] According to Bersuker,[68] Mn ions in the B sublattice of the ABO_3 perovskite structure, in principle, can possess local polar displacements for all possible valence states (for only d^3 and d^4 in the low-spin configuration). That is why we do not focus on revealing the valence state of manganese in our work. However, the emergence of the ferroelectric instability in the most common Mn^{4+} state in B-substituted STO (Ti^{4+}/Mn^{4+} ionic radius ratio of ∼1.14) can be considered by analogy with multiferroic behavior in solid solutions (Ca, Ba)MnO_3[70] and (Sr, Ba)MnO_3[71] or in $CaMnO_3$ at a negative pressure.[72] Note that for the Mn^{3+} state, the Jahn−Teller effect can manifest itself through ⟨100⟩-type distortions of the $Mn^{3+}O_6$ complex possessing tetragonal minima of the adiabatic potential energy. However, this type of distortion is not polar in systems with an inversion center, unlike in the case of the pseudo-Jahn−Teller effect, and it does not correspond to the experimentally observed structure with Mn in an off-center position (Figure 1c−f).[73]

In summary, we have discovered displacement disorder of Mn ions in the B sublattice of the $SrTiO_3$ structure. On the basis of the results of X-ray single-crystal diffraction, we established with a very high degree of accuracy ($R \sim 1\%$, and GOF ∼ 1.2) that Mn ions randomly occupy (with an occupancy of $^1/_6$) positions shifted along the ⟨001⟩ direction by 0.31 Å from central position at room temperature. Upon cooling toward the antiferrodistortive transition temperature, the off-center Mn position splits into two nonequivalent off-center positions that match the symmetry relations for the $Pm\bar{3}m \rightarrow I4/mcm$ phase transition considering the structural domain orientations. The observed octahedra tilt control of the redistribution of the Mn position provides a structural background for the temperature-activated hopping of Mn ions as the most probable mechanism of dielectric relaxation in B-substituted STO:Mn. The existence of two crystallographically nonequivalent off-center positions is at the origin of the unequal potential barrier's height distribution for possible local hopping of Mn ions. Analysis of the dielectric RF response reveals two Arrhenius-type relaxation processes characterized by similar activation energies (35 and 43 meV) and attempt frequencies (1×10^{11} and $\sim 1.6 \times 10^{10}$ Hz), suggesting the same mechanism determines the relaxation processes. We relate this mechanism with the temperature-activated hopping of Mn ions between unequal potential energy minima originating from the observed displacement disorder. The obtained results allow us to associate the dielectric relaxation in STO:Mn with the temperature-activated hopping of Mn ions, the mechanism that was reliably confirmed for A-substituted STO but is usually overlooked in B-substituted samples. To the best of our knowledge, this is the first time that an off-center position of Mn in B-substituted $SrTiO_3$ has been reported, which expands our understanding of the dielectric and possible multiferroic properties of quantum materials.

EXPERIMENTAL METHODS

Crystal Growth. $SrTiO_3$:Mn single crystals were grown by a crucible-less zone melting method with optical heating on a URN-2-ZP setup described elsewhere.[74,75] Zone recrystallization of $SrO{\cdot}TiO_2$ and $0.98SrO{\cdot}TiO_2{\cdot}0.01Mn_2O_3$ ceramic rods was carried out in air at a linear rate of 10−15 mm/h and a rod rotation rate of 40−100 rpm. The choice of Mn concentration (2 atom %) is due to the importance of further comparison with the literature data and the fact that this is the lowest possible composition where it is possible to find reliable structure−property correlations using X-ray diffraction. For the synthesis of crystals, the following reagents were used: $SrCO_3$ (99%), TiO_2 (98%), and Mn_2O_3 (96%), as well as $SrTiO_3$ single crystals as a seed, previously grown by zone melting. As a result, single-crystal cylindrical boules up to 10 mm long and up to 8 mm in diameter were obtained. The boules were transparent in the visible range and had a light yellow color for a nominally pure crystal and a burgundy color when Mn atoms were added to the crystals (Figure S3). The powder diffraction pattern of the crushed crystals, recorded on a DRON X-ray diffractometer (Cu Kα radiation), confirms that at room temperature they belong to the cubic phase of STO without any traces of impurity phases (Figure S4).

Single-Crystal X-ray Diffraction. A single crystal with developed faces and linear dimensions of 0.134 mm × 0.094 mm × 0.077 mm was selected (Figure S5) for X-ray diffraction analysis. Experimental sets of X-ray diffraction data were collected on single-crystal diffractometers (Bruker D8 QUEST at 100 K and Bruker APEX II with detector PHOTON II at 296 K) (graphite monochromatic Mo Kα radiation; λ = 0.71073 Å; φ and ω scanning) by using a single crystal. Integration of X-ray diffraction peak intensities was carried out using SAINT version 8.38A. SADABS version 2016/2 included in the APEX3 package[76] was used to take into account the absorption by crystal habits and reduce the integral intensities to a uniform scale. The crystal structure was determined using the Bruker SHELXTL APEX3 software package;[76,77] XPREP was used to determine the space group, and XT and XL were used to determine the structure and further refinement, respectively. Structural refinements were performed by full-matrix least squares over $F^2(hkl)$ with structural factors for ions Sr^{2+}, Ti^{4+}, Mn, and O^{2-}. Comparative crystal chemical analysis of possible schemes of Mn incorporation (together with literature data)[34−36,38−42] reveals the principal possibility of substitutions in B (for 3+ and 4+ valence states) and A (for the 2+ valence state) perovskite sublattices (Table S1). When considering the valence states of Mn ions, both 3+ and 4+ give similar results within the accuracy of the method, while the use of 2+ Mn (substitution in the A sublattice) led to a significant deterioration compared to substitutions in the B sublattice. The thermal parameters for all atoms were refined in the anisotropic approximation, except for the Mn atom, which was refined in the isotropic approximation. Table 1 shows the parameters of the X-ray diffraction experiment and the final results of crystal structure refinements.

https://doi.org/10.1021/acs.jpclett.2c03513
J. Phys. Chem. Lett. 2022, 13, 11720−11728

Dielectric Measurements. For dielectric RF measurements, the base surfaces of the sample were covered by the electrodes that were obtained by burning Ag paste at ∼773 K. The low-frequency complex dielectric permittivity [$\varepsilon^*(\nu) = \varepsilon'(\nu) + i\varepsilon''(\nu)$] and loss tangent [$\tan \delta(\nu) = \varepsilon''(\nu)/\varepsilon'(\nu)$] were measured at frequencies from 25 Hz to 1 MHz and temperatures from 4.2 to 294 K using a model E7-20 immittance meter (Minsk Scientific Research Instrument Making Institute, Minsk, Belarus). The temperature rate and applied ac electric field were ∼3.3 K/min and ∼1.14 V/mm, respectively. To examine the ferroelectric soft mode behavior, terahertz measurements of real $\varepsilon'(\nu)$ and imaginary $\varepsilon''(\nu)$ permittivity were performed using the TeraView TPS Spectra 3000 time domain spectrometer in transmission geometry mode on a plane-parallel 620 μm thick sample at frequencies of 5−25 cm^{-1} and temperatures of 100−300 K; below 100 K, the transmissivity was too low to allow reliable determination.

■ ASSOCIATED CONTENT

Supporting Information

The Supporting Information is available free of charge at https://pubs.acs.org/doi/10.1021/acs.jpclett.2c03513.

Shannon ionic radii, a review of Arrhenius-type dielectric relaxation, temperature dependencies of the cubic (pseudocubic) unit cell parameter, atomic displacements, distortion amplitudes, splitting of Wyckoff position 6*f*, terahertz spectra of a $SrTiO_3$ single crystal doped with Mn (2 atom %), a photo of the single crystal, X-ray powder diffraction pattern, photos of single crystals used for X-ray single-crystal diffraction analysis (PDF)

■ AUTHOR INFORMATION

Corresponding Author

Mikhail V. Talanov − *Research Institute of Physics, Southern Federal University, 344090 Rostov-on-Don, Russia;* orcid.org/0000-0002-5416-9579; Email: mvtalanov@gmail.com

Authors

Adam I. Stash − *A. N. Nesmeyanov Institute of Organoelement Compounds of Russian Academy of Science, 119991 Moscow, Russia*

Sergey A. Ivanov − *Chemical Department, Moscow State University, 119991 Moscow, Russia*

Elena S. Zhukova − *Laboratory of Terahertz Spectroscopy, Center for Photonics and 2D Materials, Moscow Institute of Physics and Technology (National Research University), Dolgoprudny, Moscow Region 141700, Russia;* orcid.org/0000-0002-5482-9477

Boris P. Gorshunov − *Laboratory of Terahertz Spectroscopy, Center for Photonics and 2D Materials, Moscow Institute of Physics and Technology (National Research University), Dolgoprudny, Moscow Region 141700, Russia*

Boris M. Nekrasov − *Laboratory of Terahertz Spectroscopy, Center for Photonics and 2D Materials, Moscow Institute of Physics and Technology (National Research University), Dolgoprudny, Moscow Region 141700, Russia;* orcid.org/0000-0003-3324-2893

Vasily S. Stolyarov − *Center for Advanced Mesoscience and Nanotechnology, Moscow Institute of Physics and Technology (National Research University), Dolgoprudny, Moscow Region 141700, Russia;* orcid.org/0000-0002-5317-0818

Vladislav I. Kozlov − *Research Institute of Solid-State Electronics Materials, MIREA - Russian Technological University (RTU MIREA), 119454 Moscow, Russia; Kapitza Institute for Physical Problems RAS, 119334 Moscow, Russia*

Maxim Savinov − *Institute of Physics, Czech Academy of Sciences, 18200 Prague, Czech Republic*

Alexander A. Bush − *Research Institute of Solid-State Electronics Materials, MIREA - Russian Technological University (RTU MIREA), 119454 Moscow, Russia*

Complete contact information is available at: https://pubs.acs.org/10.1021/acs.jpclett.2c03513

Notes

The authors declare no competing financial interest.

■ ACKNOWLEDGMENTS

The authors acknowledge D. Nuzhny for fruitful discussions and A. Melentev for assistance with terahertz experiments. This study was funded by the Russian Science Foundation via Research Projects 21-12-00358 (RF, THz, and IR experiments, crystal growth), 22-72-10022 (theoretical approaches), and 22-13-00122 (structural investigations). A.I.S., working within the government statements for the Nesmeyanov Institute of Organoelement Compounds of the Russian Academy of Sciences, is grateful to the Ministry of Science and Higher Education of the Russian Federation (Contract/Agreement 075-00697-22-00).

■ REFERENCES

(1) Müller, K. A.; Burkard, H. $SrTiO_3$: An Intrinsic Quantum Paraelectric Below 4 K. *Phys. Rev.* **1979**, *19*, 3593−3602.

(2) Kvyatkovskii, O. E. Quantum Effects in Incipient and Low-temperature Ferroelectrics (a review). *Phys. Solid State* **2001**, *43*, 1401−1419.

(3) Rupprecht, G.; Bell, R. O. Microwave Losses in Strontium Titanate above the Phase Transition. *Phys. Rev.* **1962**, *125*, 1915−1920.

(4) Vendik, O. G.; Hollmann, E. K.; Kozyrev, A. B.; Prudan, A. M. Ferroelectric Tuning of Planar and Bulk Microwave Devices. *J. supercond.* **1999**, *12*, 325−338.

(5) Tagantsev, A. K.; Sherman, V. O.; Astafiev, K. F.; Venkatesh, J.; Setter, N. Ferroelectric Materials for Microwave Tunable Applications. *J. Electroceram.* **2003**, *11*, 5−66.

(6) Li, M.; Zhou, Y.; Chen, Y.; Yang, R.; Wei, X.; Wang, S.; Jin, K. Effect of Rare Earth Elements at Amorphous $ReAlO_3/SrTiO_3$ (Re = La, Pr, Nd, Sm, Gd, and Tm) Heterointerfaces. *J. Phys. Chem. Lett.* **2021**, *12*, 1657−1663.

(7) Bugallo, D.; Langenberg, E.; Carbó-Argibay, E.; Varela Dominguez, N.; Fumega, A. O.; Pardo, V.; Lucas, I.; Morellón, L.; Rivadulla, F. Tuning Coherent-Phonon Heat Transport in $LaCoO_3/SrTiO_3$ Superlattices. *J. Phys. Chem. Lett.* **2021**, *12*, 11878−11885.

(8) Yamada, K.; Suzuki, H.; Abe, R.; Saeki, A. Complex Photoconductivity Reveals How the Nonstoichiometric Sr/Ti Affects the Charge Dynamics of a $SrTiO_3$ Photocatalyst. *J. Phys. Chem. Lett.* **2019**, *10*, 1986−1991.

(9) Cheng, C.; Long, R. Charge-Compensated Doping Extends Carrier Lifetimes in SrTiO3 by Passivating Oxygen Vacancy Defects. *J. Phys. Chem. Lett.* **2021**, *12*, 12040−12047.

(10) Fleury, P. A.; Scott, J. F.; Worlock, J. M. Soft Phonon Modes and the 110 K Phase Transition in $SrTiO_3$. *Phys. Rev. Lett.* **1968**, *21*, 16−19.

(11) Shirane, G. Neutron Scattering Studies of Structural Phase Transitions at Brookhaven. *Rev. Mod. Phys.* **1974**, *46*, 437−449.
(12) Hayward, S. A.; Salje, E. K. H. Cubic-Tetragonal Phase Transition in $SrTiO_3$ Revisited: Landau Theory and Transition Mechanism. *Phase Transit.* **1999**, *68*, 501−522.
(13) Kiat, J. M.; Roisnel, T. Rietveld Analysis of Strontium Titanate in the Müller State. *J. Phys.: Condens. Matter.* **1996**, *8*, 3471−3475.
(14) Young, J.; Rondinelli, J. M. Octahedral Rotation Preferences in Perovskite Iodides and Bromides. *J. Phys. Chem. Lett.* **2016**, *7*, 918−922.
(15) Yamanaka, A.; Kataoka, M.; Inaba, Y.; Inoue, K.; Hehlen, B.; Courtens, E. Evidence for Competing Orderings in Strontium Titanate from Hyper-Raman Scattering Spectroscopy. *Europhys. Lett.* **2000**, *50*, 688−694.
(16) Salje, E. K. H.; Aktas, O.; Carpenter, M. A.; Laguta, V. V.; Scott, J. F. Domains within Domains and Walls within Walls: Evidence for Polar Domains in Cryogenic $SrTiO_3$. *Phys. Rev. Lett.* **2013**, *111*, 247603.
(17) Frenkel, Y.; Haham, N.; Shperber, Y.; Bell, Ch.; Xie, Y.; Chen, Z.; Hikita, Y.; Hwang, H. Y.; Salje, E. K. H.; Kalisky, B. Imaging and Tuning Polarity at $SrTiO_3$ Domain Walls. *Nat. Mater.* **2017**, *16*, 1203−1208.
(18) Kityk, A. V.; Schranz, W.; Sondergeld, P.; Havlik, D.; Salje, E. K. H.; Scott, J. F. Low-frequency Superelasticity and Nonlinear Elastic Behavior of $SrTiO_3$ Crystals. *Phys. Rev. B* **2000**, *61*, 946−956.
(19) Aschauer, U.; Spaldin, N. A. Competition and Cooperation Between Antiferrodistortive and Ferroelectric Instabilities in the Model Perovskite $SrTiO_3$. *J. Phys.: Condens. Matter.* **2014**, *26*, 122203.
(20) Fleury, P. A.; Worlock, J. M. Electric-Field-Induced Raman Scattering in $SrTiO_3$ and $KTaO_3$. *Phys. Rev.* **1968**, *174*, 613−623.
(21) Li, X.; Qiu, T.; Zhang, J.; Baldini, E.; Lu, J.; Rappe, A. M.; Nelson, K. A. Terahertz Field−induced Ferroelectricity in Quantum paraelectric $SrTiO_3$. *Science* **2019**, *364*, 1079−1082.
(22) Uwe, H.; Sakudo, T. Stress-induced Ferroelectricity and Soft Phonon Modes in $SrTiO_3$. *Phys. Rev.* **1976**, *13*, 271−286.
(23) Haeni, J. H.; Irvin, P.; Chang, W.; Uecker, R.; Reiche, P.; Li, Y. L.; Choudhury, S.; Tian, W.; Hawley, M. E.; Craigo, B.; et al. G. Room-temperature Ferroelectricity in Strained $SrTiO_3$. *Nature* **2004**, *430*, 758−761.
(24) Itoh, M.; Wang, R.; Inaguma, Y.; Yamaguchi, T.; Shan, Y.-J.; Nakamura, T. Ferroelectricity Induced by Oxygen Isotope Exchange in Strontium Titanate Perovskite. *Phys. Rev. Lett.* **1999**, *82*, 3540−3543.
(25) Kim, Y. S.; Kim, J.; Moon, S. J.; Choi, W. S.; Chang, Y. J.; Yoon, J.-G.; Yu, J.; Chung, J.-S.; Noh, T. W. Localized Electronic States Induced by Defects and Possible Origin of Ferroelectricity in Strontium Titanate Thin Films. *Appl. Phys. Lett.* **2009**, *94*, 202906.
(26) Klyukin, K.; Alexandrov, V. Effect of Intrinsic Point Defects on Ferroelectric Polarization Behavior of $SrTiO_3$. *Phys. Rev. B* **2017**, *95*, 035301.
(27) Bednorz, J. G.; Müller, K. A. $Sr_{1-x}Ca_xTiO_3$: An XY Quantum Ferroelectric with Transition to Randomness. *Phys. Rev. Lett.* **1984**, *52*, 2289−2292.
(28) Lemanov, V. V.; Smirnova, E. P.; Syrnikov, P. P.; Tarakanov, E. A. Phase Transitions and Glasslike Behavior in $Sr_{1-x}Ba_xTiO_3$. *Phys. Rev. B* **1996**, *54*, 3151−3157.
(29) Shirokov, V. B.; Torgashev, V. I.; Bakirov, A. A.; Lemanov, V. V. Concentration Phase Diagram of $Ba_xSr_{1-x}TiO_3$ Solid Solutions. *Phys. Rev. B* **2006**, *73*, 104116.
(30) Ang, C.; Yu, Z.; Vilarinho, P. M.; Baptista, J. L. Bi: $SrTiO_3$: A Quantum Ferroelectric and a Relaxor. *Phys. Rev. B* **1998**, *57*, 7403−7406.
(31) Bianchi, U.; Dec, J.; Kleemann, W.; Bednorz, J. G. Cluster and Domain-state Dynamics of Ferroelectric $Sr_{1-x}Ca_xTiO_3$ (x = 0.007). *Phys. Rev. B* **1995**, *51*, 8737−8746.
(32) Lemanov, V. V. Phase Transitions in $SrTiO_3$ Quantum Paraelectric with Impurities. *Ferroelectrics* **1999**, *226*, 133−146.
(33) Shvartsman, V. V.; Bedanta, S.; Borisov, P.; Kleemann, W.; Tkach, A.; Vilarinho, P. M. (Sr;Mn)TiO_3: A Magnetoelectric Multiglass. *Phys. Rev. Lett.* **2008**, *101*, 165704.
(34) Choudhury, D.; Mukherjee, S.; Mandal, P.; Sundaresan, A.; Waghmare, U. V.; Bhattacharjee, S.; Mathieu, R.; Lazor, P.; Eriksson, O.; Sanyal, B.; et al. Tuning of Dielectric Properties and Magnetism of $SrTiO_3$ by Site-Specific Doping of Mn. *Phys. Rev. B* **2011**, *84*, 125124.
(35) Zorko, A.; Pregelj, M.; Luetkens, H.; Axelsson, A.-K.; Valant, M. Intrinsic Paramagnetism and Aggregation of Manganese Dopants in $SrTiO_3$. *Phys. Rev. B* **2014**, *89*, 094418.
(36) Valant, M.; Kolodiazhnyi, T.; Arčon, I.; Aguesse, F.; Axelsson, A.-K.; Alford, N. M. The Origin of Magnetism in Mn-Doped $SrTiO_3$. *Adv. Funct. Mater.* **2012**, *22* (10), 2114−2122.
(37) Narayan, A.; Cano, A.; Balatsky, A. V.; Spaldin, N. A. Multiferroic Quantum Criticality. *Nat. Mater.* **2019**, *18* (3), 223−228.
(38) Laguta, V. V.; Kondakova, I. V.; Bykov, I. P.; Glinchuk, M. D.; Tkach, A.; Vilarinho, P. M.; Jastrabik, L. Electron Spin Resonance Investigation of Mn^{2+} Ions and their Dynamics in Mn-doped $SrTiO_3$. *Phys. Rev. B* **2007**, *76*, 054104.
(39) Maier, R. A.; Cockayne, E.; Donohue, M.; Cibin, G.; Levin, I. Substitutional Mechanisms and Structural Relaxations for Manganese in $SrTiO_3$: Bridging the Concentration Gap for Point-Defect Metrology. *Chem. Mater.* **2020**, *32*, 4651−4662.
(40) Müller, K. A. Electron Paramagnetic Resonance of Manganese IV in $SrTiO_3$. *Phys. Rev. Lett.* **1959**, *2* (8), 341−343.
(41) Azamat, D. V.; Dejneka, A.; Lancok, J.; Trepakov, V. A.; Jastrabik, L.; Badalyan, A. G. Electron Paramagnetic Resonance Studies of Manganese Centers in $SrTiO_3$: Non-Kramers Mn^{3+} Ions and Spin-Spin Coupled Mn^{4+} Dimers. *J. Appl. Phys.* **2012**, *111* (10), 104119.
(42) Tkach, A.; Vilarinho, P. M.; Kholkin, A. L. Dependence of Dielectric Properties of Manganese-Doped Strontium Titanate Ceramics on Sintering Atmosphere. *Acta Mater.* **2006**, *54*, 5385−5391.
(43) Tkach, A.; Vilarinho, P. M.; Kholkin, A. L. Structure−Microstructure−Dielectric Tunability Relationship in Mn-doped Strontium Titanate Ceramics. *Acta Mater.* **2005**, *53*, 5061−5069.
(44) Tkach, A.; Vilarinho, P. M.; Nuzhnyy, D.; Petzelt, J. Sr- and Ti-site Substitution, Lattice Dynamics, and Octahedral Tilt Transition Relationship in $SrTiO_3$:Mn Ceramics. *Acta Mater.* **2010**, *58*, 577−582.
(45) Savinov, M.; Trepakov, V. A.; Syrnikov, P. P.; Železný, V.; Pokorný, J.; Dejneka, A.; Jastrabík, L.; Galinetto, P. Dielectric Properties of Mn doped $SrTiO_3$. *J. Phys.: Condens. Matter* **2008**, *20*, 095221.
(46) Lemanov, V. V.; Sotnikov, A. V.; Smirnova, E. P.; Weihnacht, M. Dielectric relaxation in doped $SrTiO_3$: Transition from Classical Thermal Activation to Quantum Tunnelling. *J. Appl. Phys.* **2005**, *98*, 056102.
(47) Lemanov, V. V.; Smirnova, E. P.; Sotnikov, A. V.; Weihnacht, M. Dielectric Relaxation in $SrTiO_3$: Mn. *Phys. Sol. State.* **2004**, *46*, 1442−1448.
(48) Tkach, A.; Vilarinho, P. M.; Kholkin, A. L.; Pashkin, A.; Veljko, S.; Petzelt, J. Broad-band Dielectric Spectroscopy Analysis of Relaxational Dynamics in Mn-doped $SrTiO_3$ Ceramics. *Phys. Rev. B* **2006**, *73*, 104113.
(49) Levin, I.; Krayzman, V.; Woicik, J. C.; Tkach, A.; Vilarinho, P. M. X-ray Absorption Fine Structure Studies of Mn Coordination in Doped Perovskite $SrTiO_3$. *Appl. Phys. Lett.* **2010**, *96*, 052904.
(50) Lebedev, A. I.; Sluchinskaya, I. A.; Erko, A.; Kozlovskii, V. F. Direct Evidence for Off-Centering of Mn Impurity in $SrTiO_3$. *JETP Lett.* **2009**, *89* (9), 457−460.
(51) Kvyatkovskii, O. E. Ab Initio Calculations of the Geometry and Electronic Structure of Point Defects in Ferroelectrics with a Perovskite Structure. *Phys. Sol. State.* **2009**, *51* (5), 982−990.
(52) Orobengoa, D.; Capillas, C.; Aroyo, M. I.; Perez-Mato, J. M. AMPLIMODES: Symmetry-mode Analysis on the Bilbao Crystallographic Server. *J. Appl. Crystallogr.* **2009**, *42*, 820−833.

https://doi.org/10.1021/acs.jpclett.2c03513
J. Phys. Chem. Lett. 2022, 13, 11720−11728

(53) Igartua, J. M.; Aroyo, M. I.; Kroumova, E.; Perez-Mato, J. M. Search for Pnma Materials with High-temperature Structural Phase Transitions. *Acta Crystallogr., Sect. B: Struct. Sci.* **1999**, *55*, 177−185.
(54) Talanov, M. V.; Bush, A. A.; Sirotinkin, V. P.; Kozlov, V. I. Structural Origin of Strongly Diffused Ferroelectric Phase Transition in Ba(Ti, Zr)O_3-based Ceramics. *Acta Materialia.* **2022**, *227*, 117734.
(55) Abramov, Yu. A.; Tsirelson, V. G.; Zavodnik, V. E.; Ivanov, S. A.; Brown, I. D. The Chemical Bond and Atomic Displacements in $SrTiO_3$ from X-ray Diffraction Analysis. *Acta Crystallogr., Sect. B* **1995**, *51*, 942−951.
(56) Wu, Y.-N.; Saidi, W. A.; Wuenschell, J. K.; Tadano, T.; Ohodnicki, P.; Chorpening, B.; Duan, Y. Anharmonicity Explains Temperature Renormalization Effects of the Band Gap in $SrTiO_3$. *J. Phys. Chem. Lett.* **2020**, *11*, 2518−2523.
(57) Wondratschek, H.; Müller, U.*International Tables for Crystallography*; Kluwer Academic Publishers: Dordrecht, The Netherlands, 2006; Vol. *A1*, p 731.
(58) Kroumova, E.; Perez-Mato, J. M.; Aroyo, M. I. WYCKSPLIT: a Computer Program for Determination of the Relations of Wyckoff Positions for a Group-Subgroup Pair. *J. Appl. Crystallogr.* **1998**, *31*, 646.
(59) Barrett, J. H. Dielectric Constant in Perovskite Type Crystals. *Phys. Rev.* **1952**, *86* (1), 118.
(60) Viana, R.; Lunkenheimer, P.; Hemberger, J.; Böhmer, R.; Loidl, A. Dielectric spectroscopy in $SrTiO_3$. *Phys. Rev. B* **1994**, *50*, 601−604.
(61) Levin, I.; Yang, F.; Maier, R.; Laws, W. J.; Keeble, D. S.; Cibin, G.; Sinclair, D. C. Displacive Order-Disorder Behavior and Intrinsic Clustering of Lattice Distortions in Bi-substituted $NaNbO_3$. *Adv. Funct. Mater.* **2020**, *30* (30), 2001840.
(62) Levin, I.; Keeble, D. S.; Cibin, G.; Playford, H. Y.; Eremenko, M.; Krayzman, V.; Laws, W. J.; Reaney, I. M. Nanoscale Polar Heterogeneities and Branching Bi-Displacement Directions in $K_{0.5}Bi_{0.5}TiO_3$. *Chem. Mater.* **2019**, *31* (7), 2450−2458.
(63) Radosavljevic, I.; Evans, J. S. O.; Sleight, A. W. Synthesis and Structure of Pyrochlore-Type Bismuth Titanate. *J. Solid State Chem.* **1998**, *136*, 63−66.
(64) Avdeev, M.; Haas, M. K.; Jorgensen, J. D.; Cava, R. J. Static Disorder from Lone-Pair Electrons in $Bi_{2-x}M_xRu_2O_{7-y}$ (M = Cu, Co; x = 0, 0.4) Pyrochlores. *J. Solid State Chem.* **2002**, *169*, 24−34.
(65) Bush, A. A.; Talanov, M. V.; Stash, A. I.; Ivanov, S. A.; Kamentsev, K. E. Relaxor-like Behavior and Structure Features of $Bi_2Ti_2O_7$ Pyrochlore Single Crystals. *Cryst. Growth Des.* **2020**, *20*, 824−831.
(66) Ahmed, A.; Prokhorov, A. S.; Anzin, V.; Vinnik, D.; Ivanov, S. A.; Stash, A.; Chen, Y.S.; Bush, A.; Gorshunov, B.; Alyabyeva, L. Terahertz-Infrared Dielectric Properties of Lead-Aluminum Double-Cation Substituted Single-Crystalline Barium Hexaferrite. *J. Alloys Compd.* **2022**, *898*, 162761.
(67) Pasciak, M.; Welberry, T. R.; Kulda, J.; Leoni, S.; Hlinka, J. Dynamic Displacement Disorder of Cubic $BaTiO_3$. *Phys. Rev. Lett.* **2018**, *120* (16), 167601.
(68) Bersuker, I. B. Pseudo Jahn-Teller Origin of Perovskite Multiferroics, Magnetic-Ferroelectric Crossover, and Magnetoelectric Effects: The d^0-d^{10} Problem. *Phys. Rev. Lett.* **2012**, *108*, 137202.
(69) Garcia-Fernandez, P.; Aramburu, J. A.; Barriuso, M. T.; Moreno, M. Key Role of Covalent Bonding in Octahedral Tilting in Perovskites. *J. Phys. Chem. Lett.* **2010**, *1*, 647−651.
(70) Bhattacharjee, S.; Bousquet, E.; Ghosez, P. Engineering Multiferroism in $CaMnO_3$. *Phys. Rev. Lett.* **2009**, *102*, 117602.
(71) Sakai, H.; Fujioka, J.; Fukuda, T.; Okuyama, D.; Hashizume, D.; Kagawa, F.; Nakao, H.; Murakami, Y.; Arima, T.; Baron, Q. R.; et al. Displacement-type Ferroelectric Transition with Magnetic Mn ions in Perovskite $Sr_{1-x}Ba_xMnO_3$. *Phys. Rev. Lett.* **2011**, *107*, 137601.
(72) Barone, P.; Kanungo, S.; Picozzi, S.; Saha-Dasgupta, T. Mechanism of Ferroelectricity in d^3 Perovskites: A Model Study. *Phys. Rev. B* **2011**, *84*, 134101.
(73) Bersuker, I. B. Jahn-Teller and Pseudo-Jahn-Teller Effects: From Particular Features to General Tools in Exploring Molecular and Solid State Properties. *Chem. Rev.* **2021**, *121*, 1463.
(74) Balbashov, A. M.; Egorov, S. K. Apparatus for Growth of Single Crystals of Oxide Compounds by Floating Zone Melting with Radiation Heating. *J. Cryst. Growth.* **1981**, *52*, 498−504.
(75) Balbashov, A. M.; Karabashev, S. G.; Nygmatulin, A. S. Floating Zone Melting Preparation of $YBa_2Cu_3O_{7-x}$, $YBa_2Cu_4O_{8-x}$ and $Bi_2Sr_2CaCu_2O_{8+\square}$ High-Tc Superconductor. *Prog. High Temp. Supercond.* **1989**, *24*, 95−106.
(76) *APEX3, SAINT, and SADABS*; Bruker AXS Inc.: Madison, WI, 2019.
(77) Sheldrick, G. M. Crystal Structure Refinement with SHELXL. *Acta Crystallogr.* **2015**, *C71*, 3−8.

https://doi.org/10.1021/acs.jpclett.2c03513
J. Phys. Chem. Lett. 2022, 13, 11720−11728